Published in final edited form as:
Phys Med Biol. 2013 June 21; 58(12): 4099–4118. doi:10.1088/0031-9155/58/12/4099.

Dedicated breast CT: Geometric design considerations to maximize posterior breast coverage

Srinivasan Vedantham, **Andrew Karellas**, **Margaret M Emmons**, **Lawrence J Moss**, **Sarwat Hussain**, and **Stephen P Baker**
Department of Radiology, University of Massachusetts Medical School, Worcester MA 01655 USA

Abstract

An Institutional Review Board-approved protocol was used to quantify breast tissue inclusion in 52 women, under conditions simulating both craniocaudal (CC) and mediolateral oblique (MLO) views in mammography, dedicated breast CT in the upright subject position, and dedicated breast CT in the prone subject position. Using skin as a surrogate for the underlying breast tissue, the posterior aspect of the breast that is aligned with the chest-wall edge of the breast support in a screen-film mammography system was marked with the study participants positioned for CC and MLO views. The union of skin marks with the study participants positioned for CC and MLO views was considered to represent chest-wall tissue available for imaging with mammography and served as the reference standard. For breast CT, a prone stereotactic breast biopsy unit and a custom-fabricated barrier were used to simulate conditions during prone and upright breast CT, respectively. For the same breast marked on the mammography system, skin marks were made along the breast periphery that was just anterior to the apertures of the prone biopsy unit and the upright barrier. The differences in skin marks between subject positioning simulating breast CT (prone, upright) and mammography were quantified at six anatomic locations. For each location, at least one study participant had skin mark from breast CT (prone, upright) posterior to mammography. However for all study participants, there was at least one anatomic location where the skin mark from mammography was posterior to that from breast CT (prone, upright) positioning. The maximum amount by which the skin mark from mammography was posterior to breast CT (prone and upright) over all six locations was quantified for each study participant and pair-wise comparison did not exhibit statistically significant difference between prone and upright breast CT (paired t- test, p=0.4). Quantitatively, for 95% of the study participants the skin mark from mammography was posterior to breast CT (prone or upright) by at the most 9 mm over all six locations. Based on the study observations, geometric design considerations targeting chest-wall coverage with breast CT equivalent to mammography, wherein part of the x-ray beam images through the swale during breast CT are provided. Assuming subjects can extend their chest in to a swale, the optimal swale-depth required to achieve equivalent coverage with breast CT images as mammograms for 95% of the subjects varies in the range of ~30–50 mm for clinical prototypes and was dependent on the system geometry.

Keywords

Computed tomography; Mammography; Breast CT

srinivasan.vedantham@umassmed.edu.

1. Introduction

Mammography provides a two-dimensional (2-D) image of a three-dimensional (3-D) breast resulting in tissue superposition that can potentially mask or mimic abnormalities. Dedicated breast CT provides 3-D images of the breast thus overcoming this issue. It can be performed without breast compression and can provide improved contrast (Boone et al., 2001). While dedicated breast CT was investigated in the late 1970's (Chang et al., 1979), limitations with the technology available at that time resulted in high radiation dose and poor image resolution, impeding its clinical translation (Muller et al., 1983, Raptopoulos et al., 1996). The development of flat-panel detectors has prompted reconsideration of the clinical potential of dedicated breast CT. Clinical prototype systems have been developed and early clinical trials with and without contrast media have been reported (Lindfors et al., 2008, Prionas et al., 2010, O'Connell et al., 2010, Vedantham et al., 2012b). Several research groups are exploring further improvements to dedicated breast CT (Glick et al., 2002, Thacker and Glick, 2004, Pani et al., 2004, Zeng et al., 2006, Lai et al., 2007, Madhav et al., 2009, Russo et al., 2010, Shikhaliev and Fritz, 2011, Kalender et al., 2012, Mettivier et al., 2012, Vedantham et al., 2012a, Vedantham et al., 2013, Shi et al., 2013, Chen et al., 2013). In addition, dedicated SPECT/CT and PET/CT systems for breast imaging are being developed (Brzymialkiewicz et al., 2006, Bowen et al., 2009, Mettivier et al., 2011).

One concern is the adequacy of posterior breast tissue imaged with breast CT. Lindfors et al (Lindfors et al., 2008) reported that the pectoralis musculature was visualized in 18% of the patients and visualization of axillary tail of the breast was limited. Subsequently, the design of the patient support table was refined. A recent article from the same group (Huang et al., 2011) reported that the pectoralis muscle was visualized in 85 out of 210 (40%) women. O'Connell et al (O'Connell et al., 2010) used a different breast CT clinical prototype and evaluation of imaged tissue in 40 breasts indicated statistically significant improvements in the lateral, medial, and posterior aspects, and did not observe statistically significant improvement in the inferior aspect, with breast CT compared to mammography. They observed visualization of pectoralis muscle in the superior aspect of the breast in all cases. However, in terms of visualization of lymph nodes in the axillary region, they observed statistically significant improvement with mammography than breast CT. In an independent study, Vedantham et al (Vedantham et al., 2012b) reported that the pectoralis muscle was visible in 107 out of 137 (78%) breast volumes.

At present it is unknown if the observed limitations in breast CT coverage are caused by inadequate access to breast tissue due to body habitus or due to known technical limitations of the clinical prototypes used in prior studies. The specifications of the flat-panel detector (4030CB, Varian Medical Systems) used in aforementioned clinical studies indicate an inactive region of 34 mm along the chest-wall. In comparison, flat-panel detectors used for mammography (e.g., ASX-2430, Analogic Corporation) are specified with an inactive region of 4 mm or less along the chest-wall. Hence, there are known technical limitations that could contribute to reduction in posterior breast coverage. An important question that is yet unanswered is, even if these technical limitations are overcome, would there be a reduction in posterior coverage with breast CT? Hence using skin as a surrogate for the underlying breast tissue, this study was conducted to determine if the skin marks from mammography were posterior to breast CT and to quantify the difference in skin marks between mammography and breast CT. In addition, the study also investigated breast CT using upright subject positioning as opposed to prone positioning that is currently used in clinical prototypes. An upright breast CT system could provide several attractive features including a small footprint enabling its installation in rooms that house mammography and digital breast tomosynthesis units, and potentially easier positioning of the patient.

2. Materials and Methods

2.1. Subjects

Fifty-two subjects, all women, participated in the study that was conducted in adherence to a protocol approved by our institutional review board and written informed consent was obtained from all study participants. The inclusion criterion was that all study participants should be women of at least 40 years of age as this represents the characteristics of subjects routinely screened for breast cancer. Male subjects, pregnant women, women who had bilateral mastectomies and did not undergo reconstructive surgery, and women who were frail that limited them from standing upright or were uncomfortable lying prone on a table were excluded. All measurements were performed by a single mammography-certified radiologic technologist for consistency. Study participants did not undergo imaging as part of this research study.

2.2. Body habitus measurements

Age, height, weight, prior history of breast surgery and its nature, cup size of frequently used bra, and demographic information were verbally obtained from each study participant and recorded in the study form by the mammography-certified technologist. The technologist measured the circumference of the chest superior to the breast, the circumference of the chest inferior to the breast, chin to nipple vertical distance, and nipple to umbilicus vertical distance, using a flexible tape measure with the participant standing upright. Each study participant chose left or right breast and all measurements including skin marks for quantifying coverage were performed on the same breast. The study was conducted at a site that was primarily a diagnostic facility and the study participants were allowed to choose breast laterality as some of the study participants might have undergone procedures that may have caused discomfort. The technologist also measured the circumference of the chosen breast at the chest-wall using a circular ring scale in a manner similar to that described by Boone et al (Boone et al., 2004). Assuming that the cross-section of the breast at the chest-wall can be approximated by a circle, the diameter of the breast at the chest-wall was computed from its circumference.

2.3. Skin marking with mammography

The small (18 cm × 24 cm) and large (24 cm × 30 cm) compression paddles of a screen-film mammography unit (Senographe 800T, GE Healthcare) were machined at the chest-wall edge to provide a 5-mm wide slot (Figure 1). Each study participant was positioned for the cranio-caudal (CC) view and prior to breast compression the chest-wall to nipple distance was measured. After mild breast compression (approximately 5 daN), the skin was marked through the slot in the compression paddle as a continuous line using a single-use, sterile, surgical skin marker with 0.5 mm tip. The inferior aspect of the breast (infra-mammary fold) was marked at the edge of the breast support. After positioning each study participant for the medio-lateral oblique (MLO) view, the skin along the medial and superior aspects of the breast was marked through the slot in the compression paddle in a manner similar to the CC view. The lateral aspect of the breast extending to the axilla was marked at the edge of the breast support plate during the MLO view. Different colour skin markers were used for patient positioning that simulated mammography, breast CT with prone subject positioning, and breast CT with upright subject positioning to aid in identification.

2.4. Skin marking with simulated prone breast CT

A prone stereotactic breast biopsy table (Multicare Platinum, Hologic, Inc.) was used to simulate patient positioning in a prone breast CT system. The table featured a 23 cm (9 inch) circular aperture through which the breast was pendant. The compressible foam mattress

was not removed during the study as it represented the manner in which subjects are positioned during prone breast biopsy. The skin along the circumference of the breast that was just anterior to the aperture was marked as a continuous line using a sterile, single-use, surgical skin marker.

2.5. Skin marking with simulated upright breast CT

A custom patient-protective barrier was fabricated to simulate subject positioning with an upright breast CT system (Figure 2). The rectangular barrier (91 cm width × 61 cm height) was fabricated from 9.5 mm thick flat polycarbonate sheet and could be vertically translated to suit the height of the study participant. The barrier featured a 29 cm circular aperture and a curved breast support with a gap between the barrier and breast support to facilitate marking of the skin. The study participant was positioned to simulate an upright breast CT system with her chest against the barrier and with slight medial rotation of the torso to improve inclusion of the axillary aspects of the breast. A sterile, single-use, surgical skin marker was used to mark the skin as a continuous line along the circumference of the breast that was just anterior to the aperture.

2.6. Quantification of chest-wall tissue available for imaging

The union of skin marks made with the study participant positioned for CC and MLO views on the mammography unit was considered to be representative of chest-wall tissue available for imaging with mammography and served as reference. With respect to this reference, the differences in skin marks made with upright breast CT and prone breast CT were quantified at six locations shown in Figure 3. These locations correspond to: (1) anterior axillary line at the axilla; (2) medial and inferior attachment; (3) medial attachment; (4) lateral attachment; (5) superior attachment; and (6) inferior attachment. Among these locations, the medial and inferior attachment, the lateral attachment, and the inferior attachment were obtained from skin marks made at the posterior edge of the breast support and the remainder from skin marks made through the slot in the compression paddle. There was a mismatch between the mark made at the posterior edge of the breast support and that through the compression paddle, as the lip of the compression paddle was posterior to the breast support. Mammography systems are designed in such manner to ensure that the lip of the compression paddle is not visible on the mammograms. Hence, skin marks made through the compression paddle were corrected so that all skin marks made with mammography correspond to the posterior edge of the breast support. This correction is illustrated in Figure 4. The skin marks were not corrected to account for the inactive region between the posterior edge of the breast support and the posterior edge of the detector (first row/column of pixels) and hence, the skin marks represent chest-wall tissue *available for imaging* with mammography and not posterior tissue *imaged* in mammograms. Thus, if $s^{P}_{i,n}$, $s^{U}_{i,n}$ and $s^{M}_{i,n}$ represent the skin marks at the i-th location (i=1,2,…,6, representing the 6 anatomic locations) for the n-th study participant positioned for prone breast CT, upright breast CT, and mammography (after aforementioned correction), respectively, then the difference in skin marks between prone breast CT and mammography ($D^{P}_{i,n}$) and the difference in skin marks between upright breast CT and mammography ($D^{U}_{i,n}$) were quantified as:

$$D^{P}_{i,n}=s^{P}_{i,n}-s^{M}_{i,n}\quad D^{U}_{i,n}=s^{U}_{i,n}-s^{M}_{i,n} \qquad (1)$$

The value is positive when the skin mark from breast CT (upright, prone) is posterior to mammography and is negative when vice versa. Statistical analyses were performed either using the SPSS statistical software package (Version 15, SPSS, Inc.) or using OriginPro

(Version 8.6.0, OriginLab Corporation). Effects associated with p-values less than or equal to 0.05 were considered to be statistically significant.

3. Results

Race and ethnicity characteristics are provided in Table 1. Prior history of breast surgery was reported by 9 study participants, of which 2 study participants had breast reduction (cosmetic) surgery, 1 participant had breast augmentation (cosmetic) surgery and the remainder (6 participants) had lumpectomy. Summary of the results from the body habitus measurements performed with the study participants standing upright are provided in Table 2.

Table 3 summarize the results from measurement of breast dimensions including the circumference of the breast at the chest-wall and the chest to nipple distance, along with the frequently used bra cup size reported by the study participant. These results were obtained from measurements performed on 29 right breasts and 23 left breasts based on study participant's preference. Statistical analysis (Mann-Whitney test) indicated that there was no significant difference in circumference of the breast at chest-wall (p=0.619), chest to nipple length (p=0.684), circumference of the chest superior to the breast (p=0.173), and circumference of the chest inferior to the breast (p=0.258) with breast laterality. In terms of the bra cup size, monotonic increases in mean circumference of the breast at chest-wall and mean chest to nipple distance were observed with increasing cup size (Table 3). This observation is in agreement with a previous study (Huang et al., 2011). Tables 2 and 3 could be useful for the geometric design of a dedicated breast CT system such as the size of the aperture through which the breast is imaged and magnification, with considerations for radiation dose and image quality. The mean diameter of the breast at the chest-wall, computed from the circumference, was 14.7 cm. This is in the range reported in previous studies (Boone et al., 2004, Vedantham et al., 2012b). Statistically significant correlations (Spearman *rho*) were observed between breast dimensions and body habitus measures (Table 4). Statistically significant and positive correlation was observed between the diameter of the breast at the chest-wall and chest to nipple distance. Also, the diameter of the breast at chest-wall and the chest to nipple distance were positively correlated and statistically significant with the circumference of the chest superior to the breast and with the circumference of the chest inferior to the breast.

Figure 5 shows the box plots of the difference in skin marks at six locations between mammography and the setups simulating breast CT with (A) prone (D_i^P) and (B) upright (D_i^U) subject positioning. In Figure 5, the maxima (whisker) at each location is greater than zero indicating that for each location the skin mark from breast CT (prone or upright) was posterior to mammography for at least one study participant. Also, the minima (whisker) at each location is less than zero indicating that for each location the skin mark from mammography was posterior to breast CT (prone or upright) for at least one study participant.

The association between body habitus measures and location-dependent difference in skin marks ($D_i^{P/U}$) was determined using Spearman *rho* (Table 5). With study participants positioned for prone breast CT, statistically significant and negative correlations were observed at the lateral and superior attachments with the diameter of the breast at chest-wall, and between the superior attachment and the circumference of the chest inferior to the breast. With study participants positioned for upright breast CT, statistically significant and negative correlations were observed at the medial and inferior attachment and at the medial attachment with chin to nipple vertical distance, and statistically significant and positive

correlation was observed between the medial and inferior attachment and the nipple to umbilicus vertical distance. Thus, there is an association between body habitus measures and location-dependent difference in skin marks and this association is different for prone and upright breast CT.

While the data shown in Figure 5 provides insight into the location-dependence of chest-wall tissue available for imaging with breast CT compared to mammography, these data are likely to be correlated and this expectation is confirmed in Table 6. Hence, it is apparent that the locations cannot be treated independently. An interesting observation in Table 6 is that the statistically significant correlations (Spearman *rho*) between location pairs were different for prone and upright breast CT. Importantly, if there is reduction in chest-wall tissue with breast CT (compared to mammography) even at one location, then there will be a loss of chest-wall tissue in the reconstructed breast CT images. Thus, referring to equation (1), the minima of $D_i^{P/U}$ over i =6 locations for each study participant, represented as $\underset{i}{\mathrm{MIN}}(D_i^{P/U})$, is the appropriate metric for analysis. For study participants positioned for prone breast CT, the correlation (Spearman *rho)* between $\underset{i}{\mathrm{MIN}}(D_i^{P})$ and body habitus measures (Table 7) indicate statistically significant and negative correlations with the circumference of breast at chest-wall and the circumference of chest inferior to breast. However, for upright positioning, $\underset{i}{\mathrm{MIN}}(D_i^{U})$ did not exhibit statistically significant correlation with any of the body habitus measures studied.

Figure 6(A) shows $\underset{i}{\mathrm{MIN}}(D_i^{P})$ and $\underset{i}{\mathrm{MIN}}(D_i^{U})$ over the six locations for each study participant. For all study participants, $\underset{i}{\mathrm{MIN}}(D_i^{P})<0$ and $\underset{i}{\mathrm{MIN}}(D_i^{U})<0$ indicating that the skin mark made with the study participant positioned for mammography was posterior to that made with the study participant positioned for breast CT (prone and upright) in at least one of the six locations. Figure 6(B) shows the histograms of $\underset{i}{\mathrm{MIN}}(D_i^{P})$ and $\underset{i}{\mathrm{MIN}}(D_i^{U})$ over the six locations in 0.5 mm bins that corresponds to the tip size of the skin marker. Kolmogorov-Smirnov test indicated that the histograms of $\underset{i}{\mathrm{MIN}}(D_i^{P})$ and $\underset{i}{\mathrm{MIN}}(D_i^{U})$ did not significantly differ from a normal distribution ($p > 0.74$) . At the 0.05 level, paired t-test indicated that the means of $\underset{i}{\mathrm{MIN}}(D_i^{P})$ and $\underset{i}{\mathrm{MIN}}(D_i^{U})$ were not statistically different ($p = 0.4$). Figure 6(C) and 6(D) show the histograms, expressed in percentage of subjects, of the locations that correspond to $\underset{i}{\mathrm{MIN}}(D_i^{P})$ and $\underset{i}{\mathrm{MIN}}(D_i^{U})$, respectively. For more than 75% of the study participants $\underset{i}{\mathrm{MIN}}(D_i^{P})$ correspond to either the lateral attachment (location 4) or the anterior axillary line at the axilla (location 1). For 75% of the study participants, $\underset{i}{\mathrm{MIN}}(D_i^{U})$ corresponds to the lateral attachment (location 4). From the histograms in Figure 6(B), the cumulative distributions of the percentage of study participants for whom the skin mark from mammography positioning was posterior to breast CT positioning (prone and upright) by the specified amount represented by the threshold t was generated (Figure 7). Quantitatively, for 95% of the study participants the skin mark from mammography positioning was posterior to breast CT positioning (either prone or upright) by at the most 9 mm over all six locations. We will refer to this measure as $D_{0.95}$, and $D_{0.95}$ =9 mm. Over all study participants, the skin mark from mammography positioning was posterior to that from prone and upright breast CT positioning by at the most 11 and 10 mm, respectively, over all locations.

4. Discussion

Comparing prone and upright breast CT positioning (Figure 6) in terms of $\underset{i}{\mathrm{MIN}}(D_i^P)$ and $\underset{i}{\mathrm{MIN}}(D_i^U)$, the means were not statistically significant. However, there were differences between the two set-ups. The prone stereotactic table used in this study was curved laterally and had a dip at the region supporting the chest of the study participant, whereas the custom-fabricated barrier used to simulate an upright breast CT system had a flat surface. Additionally, the compressible foam mattress was in-place during measurements simulating prone breast CT, whereas the upright system did not need such a mattress. Further, the diameters of the circular apertures through which the breast extends were also different between prone (23 cm) and upright (29 cm) set-ups. Current experience is based on breast CT in the prone position; however, from the practical point of view, the upright approach requires less space and is desirable for installation in existing mammography facilities. Although there were differences between the upright and prone set-ups, the observation that that the means of $\underset{i}{\mathrm{MIN}}(D_i^P)$ and $\underset{i}{\mathrm{MIN}}(D_i^U)$ were not statistically different suggests that the upright approach to breast CT is an option that needs further investigation. Future work could be directed towards measurement of breast shape during upright breast CT and the effect of breast shape on radiation dose distribution.

European guidelines for quality assurance in mammography (Perry et al., 2006) indicate a limiting value of 5 mm for chest-wall missed tissue, where the measurement corresponds to the distance between the posterior edge of the breast support and the imaged area (the distance d_s in Figure 4). U.S. Food and Drug Administration regulations (FDA, 2002) stipulate that the posterior (chest-wall) edge of the compression paddle shall not extend beyond the detector by more than 1% of the source-to-detector distance when the compression paddle is at a distance equal to standard breast thickness. Quality control procedures used as part of a large clinical trial comparing digital and screen-film mammography (Bloomquist et al., 2006) used a limit of 7 mm for chest-wall missed tissue, where the measurement was in accordance with FDA regulations.

Let L^M represent the accepted limit for chest-wall missed tissue with mammography, i.e., L^M = 5 or 7 mm. Thus, the chest-wall tissue *imaged* in mammograms will be anterior to the skin marks made along the chest-wall edge of the breast support with mammography by L^M. Recalling that the computed $D_{0.95}$ =9 mm for breast CT is with respect to the skin mark at the chest-wall edge of the breast support with mammography, the geometric design of the breast CT system factoring the location of the x-ray focal spot and the detector inactive region should compensate for $D_{0.95}-L^M$ to obtain equivalent chest-wall coverage in breast CT images as mammograms. The necessary condition and the swale depth required to obtain equivalent chest-wall coverage in breast CT images as mammograms are provided below.

Let us consider a prone breast CT system, comprising a table with a swale (Figure 8) through which the breast is pendant during imaging. Let d_s^a and d_s^p represent the anterior and posterior diameters of the swale and s_d the swale-depth. In order to accommodate the largest breast represented by its diameter $d_b^{\max}$, $d_s^a \geq d_b^{\max}$. Assuming the cross-section of the breast at the chest-wall can be approximated by a circle, $d_b^{\max}$ from this study was 18.4 cm. Prior studies (Boone et al., 2004, Vedantham et al., 2012b) have reported $d_b^{\max}$ of up to 20.5 cm. In Figure 8(A), S^P is the skin mark with the subject positioned for prone breast CT. Recalling that the skin along the circumference of the breast that was just anterior to the aperture was marked with the subject positioned for prone breast CT, S^P is aligned with the anterior end of the swale. S^M is the skin mark along the posterior edge of the breast support with the subject positioned for mammography and is posterior to S^P by at the most 9 mm for

95% of study participants ($D_{0.95}$ =9 mm). The point marked by a cross is anterior to S^M by L^M, which is the accepted limit for chest-wall missed tissue in mammograms. Hence, in order for prone breast CT images to provide equivalent chest-wall coverage as mammograms, the point marked by the cross needs to be imaged. Thus, with respect to S^P, $D_{0.95} - L^M$ is the amount of breast tissue posterior to S^P that needs to be imaged so as to obtain equivalent chest-wall coverage in breast CT images as mammograms. Referring to Figure 8(B), it can be inferred that with respect to the anterior surface of the table ($z = 0$) the skin mark S^P corresponds to the swale-depth s_d. The $z-$ axis is along the axis of rotation (AOR) and $z = 0$ corresponds to the anterior surface of the table. Let x_i and x_d represent the locations of the focal spot and the first row/column of detector pixels, respectively, with respect to $z = 0$. Thus, x_t and x_d include the mechanical clearance needed to facilitate rotation of the x-ray tube- detector assembly about the AOR. Assuming circular trajectories for the x-ray tube and the detector, let r_t and r_d represent the corresponding radii. It can be readily observed that choosing $r_t \geq 0.5d_s^p$ and $r_d \geq 0.5d_s^p$ would be beneficial in reducing x_t and x_d, respectively. For prototype breast CT systems described, typically $x_t > x_d$. As an example, for one system the x-ray focal spot was located 47.5 mm from the anterior end of the x-ray tube (Boone, 2004), whereas the detector dead space is 34.2 mm. Assuming uniform mechanical clearance for the x-ray tube and detector to facilitate their rotation about the AOR, it can be observed that $x_t > x_d$. Hence, the discussion is initially restricted for the case $x_t > x_d$. The central beam is defined to be perpendicular to the $z-$ axis. With respect to the central beam, the maximum cone-angle in the posterior direction that can be imaged is denoted by $\gamma_p^{\max}$. Let γ_p^T represent the ray connecting the x-ray source to the detector through the point marked by a cross in Figure 8(B). The necessary condition is $\gamma_p^{\max} \geq \gamma_p^T$. For $\gamma < 90°$ which is trivially satisfied for the geometry shown in Figure 8B, if $\gamma_p^{\max} \geq \gamma_p^T$ then, $\tan(\gamma_p^{\max}) \geq \tan(\gamma_p^T)$. From geometry, it can be observed that this condition is satisfied when,

$$\frac{(x_t - x_d)}{(r_t - r_d)} \geq \frac{x_t - s_d + \left(D_{0.95} - L^M\right)}{r_t} \quad (2)$$

Rewriting (2) in terms of the swale-depth s_d yields,

$$s_d \geq x_t + \left(D_{0.95} - L^M\right) - r_t \left[\frac{x_t - x_d}{r_t + r_d}\right] \quad (3)$$

Corresponding to the region where the x-ray beam traverses through the swale, beam hardening artifacts could occur depending on the chosen material for the swale. Hence, minimizing the swale region through which x-ray beam traverses would be beneficial. Thus from (3), the optimal swale-depth s_d^* is:

$$s_d^* = x_t + \left(D_{0.95} - L^M\right) - \left[\frac{x_t - x_d}{M}\right] \quad (4)$$

In (4), the magnification, $M = \frac{(r_t + r_d)}{r_t}$. Since $\gamma_p^T > 0$, some portion of the breast will not be imaged in every projection, resulting in reduced image quality and this region of the breast is shown in Figure 8(C).

For the setup simulating upright breast CT, the barrier used had a flat surface. In Figure 9, the skin mark corresponding to the measurement is shown as S^U. $D_{095} - L^M$ is the amount of breast tissue posterior to S^U that needs to be imaged so as to obtain equivalent chest-wall coverage in breast CT images as mammograms for 95% of the subjects and is marked by a cross. If x_t and x_d represent the locations of the x-ray focal spot and the first row/column of the detector from the anterior surface of the barrier along z-axis, then the intersection of a ray from the x-ray focal spot to the first row/column of detector with the axis of rotation (AOR) is denoted by P. If r_t and r_d represent the radii for the x-ray source and the detector trajectories, then from geometry,

$$\frac{x_t - x_d}{r_t + r_d} = \frac{x_t - P}{r_t} \quad (5)$$

Solving for P and substituting $M = \frac{(r_t + r_d)}{r_t}$ yields,

$$P = x_t - \left[\frac{x_t - x_d}{M}\right] \quad (6)$$

The breast needs to be shifted in the anterior direction by $P + (D_{0.95} - L^M)$ so that the point marked by the cross is congruent with P. The swale-depth, s_d^* required to achieve this shift is considered optimal and can be determined as per equation (7), which is identical to equation (4).

$$s_d^* = x_t + \left(D_{0.95} - L^M\right) - \left[\frac{x_t - x_d}{M}\right] \quad (7)$$

Since, $D_{0.95}$ =9 mm was observed in this study for both upright and prone setups simulating breast CT, the optimal swale-depth for prone and upright breast CT are identical, when x_t, x_d and M are fixed. Based on geometry, equations (4) and (7) can be generalized to be also applicable when $x_d \geq x_t$ as shown in (8), where $\left| \right|$ indicates the absolute value.

$$s_d^* = \mathrm{MAX}(x_t, x_d) + \left(D_{0.95} - L^M\right) - \left|\left[\frac{x_t - x_d}{M}\right]\right| \quad (8)$$

Minimizing s_d^* is important as it would reduce the amount by which the subject has to flex her torso backwards to maximize tissue inclusion and can alleviate the discomfort (neck strain) observed in a prior study (O'Connell et al., 2010). The observed negative correlation between the circumference of the breast at the chest-wall and $\underset{i}{\mathrm{MIN}}(D_i^P)$ in Table 7 emphasizes the need for minimizing s_d^* for subjects with smaller breasts. From (8), it is apparent that reducing x_t, x_d and M would be beneficial in reducing s_d^*. While initial system designs were limited by the choice of x-ray tube and detector available at that time, there have been substantial improvements in x-ray tube and detector that allow reduction of x_t and x_d. Figure 10 shows s_d^* as a function of M for three combinations of x_t and x_d. Estimates of s_d^* were obtained assuming a uniform mechanical clearance of 5 mm for the x-ray tube and the detector and with L^M =5 mm, corresponding to European guidelines. x_t = 52.5 mm was obtained from Boone (Boone, 2004) and x_t = 37 mm was obtained from the specifications of the M-1500 x-ray tube (Varian Medical Systems), which is used in a recently installed clinical prototype at our institution and in a recent independent report (Gazi et al., 2013). x_d

= 39.2 mm and 23.6 mm, were obtained from specifications of the PaxScan® 4030CB and PaxScan® 4030MCT (Varian Medical Systems), respectively. For current clinical prototypes, M ranges from 1.42 (Sechopoulos et al., 2010) to 2.03 (Prionas et al., 2011). For M of one early prototype system (Boone, 2004), the estimated s_d^*=48.9mm. For the system geometry of a recently installed system at our institution that uses the M-1500 x-ray tube and PaxScan® 4030MCT detector, the s_d^*=31.6mm. While the data and the analysis presented were targeted for breast CT, the optimal swale-depth determined could be applicable for patient-support tables used with prone stereotactic breast biopsy systems and for the face-shield (barrier) used with digital breast tomosynthesis systems. The presented data could also be useful for helical breast CT systems, where an axial scan is performed at the chest-wall followed by a helical scan along the chest-wall to nipple direction.

This study had limitations. Skin marks were used as a surrogate metric to measure posterior breast tissue coverage due to cost considerations in fabricating prone and upright breast CT systems. The accuracy of this metric to represent the underlying breast tissue is not established. In particular, during mammographic positioning the breast is extracted from the chest-wall prior to compression. This could preferentially include more skin than the underlying tissue during mammography and could have influenced the estimate of the difference in skin marks between mammography and breast CT positioning in favor of mammography. While s_d^* is dependent on system geometry, the ability of subjects to extend their chest into a swale of given depth was not studied and will be investigated in future. It is possible that for large s_d^*, subjects may not be able to extend their chest into the imaged field of view limiting posterior coverage. Although the skin was marked continuously for the set-ups simulating mammography, prone and upright breast CT, data from six anatomic locations that were easy to identify were chosen for analysis. While these locations covered the circumference of the breast at the chest-wall, it is possible that the posterior breast tissue coverage may vary at intermediate locations. Additionally, our study did not quantify repeatability in the measurements. Even in the well-established mammography, substantial variability in the amount of posterior breast tissue imaged could be observed depending on the extent to which the breast tissue is pulled from the chest-wall during subject positioning (Kopans, 2008, ACR, 1999).

We considered alternate methods of analyzing the data from skin marks such as estimating projected area of the breast or the breast volume available for imaging. However, this would require assuming a specific shape for the breast with mammography and breast CT. While the shape of the breast in mammography and prone breast CT can be approximated, it is difficult to generalize the shape of the breast for upright breast CT. In Figure 5, for each location, at least one subject had skin marks with breast CT posterior to mammography. For such instances, additional assumption regarding the shape of the torso is also needed, if posterior coverage were to be estimated based on breast volume. Considering the uncertainties in these assumptions, the analysis presented directly utilizes the measured data.

5. Conclusion

This study investigated posterior breast coverage in dedicated breast CT by using skin as a surrogate for underlying breast tissue. The study observed an association between body habitus measures and breast dimensions. At each location, the skin mark from breast CT (prone or upright) was posterior to mammography for at least one subject. However, for each subject there was at least one location where the skin mark from mammography was posterior to breast CT (prone or upright). The maximum amount by which the skin mark from mammography was posterior to breast CT (prone and upright) over all six locations was quantified for each study participant and pair-wise comparison did not exhibit

statistically significant difference between prone and upright breast CT (paired t- test, p=0.4). Quantitatively, for 95% of the study participants the skin mark from mammography was posterior to breast CT (either prone or upright) by at the most 9 mm over all six locations. The location-dependence of the difference in skin marks between breast CT positioning and mammography was observed to be correlated with body habitus measures. Based on the measured data and assuming that subjects can extend their chest into a swale, the optimal swale-depth required to achieve equivalent coverage with breast CT images as mammograms for 95% of the subjects varies in the range of ~30–50 mm for clinical prototypes and is dependent on the system geometry including magnification, the location of the x-ray focal spot and the location of the first row/column of the detector.

Acknowledgments

This work was supported by National Institutes of Health (NIH) grant number R01 CA128906. The contents are solely the responsibility of the authors and do not represent the official views of the NIH or the National Cancer Institute (NCI). The authors thank Mr. Art Allard and Mr. Tom Partington, University of Massachusetts Medical School, for their assistance in the design and fabrication of the upright barrier. The authors thank David Conover, Koning Corporation, for providing the specifications of the M-1500 x-ray tube and the PaxScan® 4030MCT detector.

References

ACR. Mammography Quality Control Manual. Reston, VA: American College of Radiology (ACR); 1999.

Bloomquist AK, Yaffe MJ, Pisano ED, Hendrick RE, Mawdsley GE, Bright S, Shen SZ, Mahesh M, Nickoloff EL, Fleischman RC, Williams MB, Maidment AD, Beideck DJ, Och J, Seibert JA. Quality control for digital mammography in the ACRIN DMIST trial: part I. Med Phys. 2006; 33:719–736. [PubMed: 16878575]

Boone, JM. Breast CT: Its prospect for breast cancer screening and diagnosis. In: Karellas, A.; Giger, LM., editors. Advances in breast imaging: Physics, Technology and Clinical Applications, Categorical course in diagnostic radiology physics. Oak Brook, IL: Radiological Society of North America (RSNA); 2004.

Boone JM, Nelson TR, Lindfors KK, Seibert JA. Dedicated breast CT: radiation dose and image quality evaluation. Radiology. 2001; 221:657–667. [PubMed: 11719660]

Boone JM, Shah N, Nelson TR. A comprehensive analysis of DgN(CT) coefficients for pendant-geometry cone-beam breast computed tomography. Med Phys. 2004; 31:226–235. [PubMed: 15000608]

Bowen SL, Wu Y, Chaudhari AJ, Fu L, Packard NJ, Burkett GW, Yang K, Lindfors KK, Shelton DK, Hagge R, Borowsky AD, Martinez SR, Qi J, Boone JM, Cherry SR, Badawi RD. Initial characterization of a dedicated breast PET/CT scanner during human imaging. J Nucl Med. 2009; 50:1401–1408. [PubMed: 19690029]

Brzymialkiewicz CN, Tornai MP, Mckinley RL, Cutler SJ, Bowsher JE. Performance of dedicated emission mammotomography for various breast shapes and sizes. Physics in Medicine and Biology. 2006; 51:5051–5064. [PubMed: 16985287]

Chang CH, Sibala JL, Fritz SL, Dwyer SJ 3rd, Templeton AW. Specific value of computed tomographic breast scanner (CT/M) in diagnosis of breast diseases. Radiology. 1979; 132:647–652. [PubMed: 472242]

Chen L, Abbey CK, Boone JM. Association between power law coefficients of the anatomical noise power spectrum and lesion detectability in breast imaging modalities. Phys Med Biol. 2013; 58:1663–1681. [PubMed: 23422272]

FDA, U. S.. Mammography Quality Standards Act Regulations. Sec. 900.12 Quality standards.(e) Quality assurance-equipment (5) Annual quality control tests. Rockville, MD: U.S. Food and Drug Administration; 2002.

Gazi, P.; Yang, K.; Burkett, G.; Boone, JM. Development and spatial resolution characterization of a dedicated pulsed x-ray, cone-beam breast CT system. In: Nishikawa, RM.; Whiting, BR.;

Hoeschen, C., editors. Medical Imaging 2013: Physics of Medical Imaging. Vol. Vol. 8668. SPIE; 2013. p. 86681D-1

Glick, SJ.; Vedantham, S.; Karellas, A. Investigation of optimal kVp settings for CT Mammography using a Flat-panel Imager. In: Antonuk, LE.; Yaffe, JM., editors. Medical Imaging 2002: Physics of Medical Imaging. Vol. Vol. 4682. SPIE; 2002. p. 392-402.

Huang SY, Boone JM, Yang K, Packard NJ, Mckenney SE, Prionas ND, Lindfors KK, Yaffe MJ. The characterization of breast anatomical metrics using dedicated breast CT. Med Phys. 2011; 38:2180–2191. [PubMed: 21626952]

Kalender WA, Beister M, Boone JM, Kolditz D, Vollmar SV, Weigel MC. High-resolution spiral CT of the breast at very low dose: concept and feasibility considerations. Eur Radiol. 2012; 22:1–8. [PubMed: 21656331]

Kopans DB. Basic physics and doubts about relationship between mammographically determined tissue density and breast cancer risk. Radiology. 2008; 246:348–353. [PubMed: 18227535]

Lai CJ, Shaw CC, Chen L, Altunbas MC, Liu X, Han T, Wang T, Yang WT, Whitman GJ, Tu SJ. Visibility of microcalcification in cone beam breast CT: effects of X-ray tube voltage and radiation dose. Med Phys. 2007; 34:2995–3004. [PubMed: 17822008]

Lindfors KK, Boone JM, Nelson TR, Yang K, Kwan AL, Miller DF. Dedicated breast CT: initial clinical experience. Radiology. 2008; 246:725–733. [PubMed: 18195383]

Madhav P, Crotty DJ, Mckinley RL, Tornai MP. Evaluation of tilted cone-beam CT orbits in the development of a dedicated hybrid mammotomograph. Phys Med Biol. 2009; 54:3659–3676. [PubMed: 19478374]

Mettivier G, Russo P, Cesarelli M, Ospizio R, Passeggio G, Roscilli L, Pontoriere G, Rocco R. Dedicated scanner for laboratory investigations on cone-beam CT/SPECT imaging of the breast. Nuclear Instruments & Methods in Physics Research Section a-Accelerators Spectrometers Detectors and Associated Equipment. 2011; 629:350–356.

Mettivier G, Russo P, Lanconelli N, Meo SL. Cone-beam breast computed tomography with a displaced flat panel detector array. Med Phys. 2012; 39:2805–2819. [PubMed: 22559652]

Muller JWT, Vanwaes PFGM, Koehler PR. Computed-Tomography of Breast-Lesions - Comparison with X-Ray Mammography. J Comput Assist Tomogr. 1983; 7:650–654. [PubMed: 6863666]

O'Connell A, Conover DL, Zhang Y, Seifert P, Logan-Young W, Lin CF, Sahler L, Ning R. Cone-beam CT for breast imaging: Radiation dose, breast coverage, and image quality. AJR Am J Roentgenol. 2010; 195:496–509. [PubMed: 20651210]

Pani S, Longo R, Dreossi D, Montanari F, Olivo A, Arfelli F, Bergamaschi A, Poropat P, Rigon L, Zanconati F, Dalla Palma L, Castelli E. Breast tomography with synchrotron radiation: preliminary results. Phys Med Biol. 2004; 49:1739–1754. [PubMed: 15152928]

Perry, N.; Broeders, M.; De Wolf, C.; Tornberg, S.; Holland, R.; Von Karsa, L.; Puthaar, E., editors. European guidelines for quality assurance in breast cancer screening and diagnosis. Fourth Edition. Luxembourg: Office for Official Publications of the European Communities; 2006.

Prionas ND, Huang SY, Boone JM. Experimentally determined spectral optimization for dedicated breast computed tomography. Med Phys. 2011; 38:646–655. [PubMed: 21452702]

Prionas ND, Lindfors KK, Ray S, Huang SY, Beckett LA, Monsky WL, Boone JM. Contrast-enhanced dedicated breast CT: initial clinical experience. Radiology. 2010; 256:714–723. [PubMed: 20720067]

Raptopoulos V, Baum JK, Hochman M, Karellas A, Houlihan MJ, D'Orsi CJ. High resolution CT mammography of surgical biopsy specimens. J Comput Assist Tomogr. 1996; 20:179–184. [PubMed: 8606220]

Russo P, Mettivier G, Lauria A, Montesi MC. X-ray Cone-Beam Breast Computed Tomography: Phantom Studies. Ieee Transactions on Nuclear Science. 2010; 57:160–172.

Sechopoulos I, Feng SS, D'Orsi CJ. Dosimetric characterization of a dedicated breast computed tomography clinical prototype. Med Phys. 2010; 37:4110–4120. [PubMed: 20879571]

Shi L, Vedantham S, Karellas A, O'Connell AM. Technical Note: Skin thickness measurements using high-resolution flat-panel cone-beam dedicated breast CT. Med Phys. 2013; 40:031913. [PubMed: 23464328]

Shikhaliev PM, Fritz SG. Photon counting spectral CT versus conventional CT: comparative evaluation for breast imaging application. Phys Med Biol. 2011; 56:1905–1930. [PubMed: 21364268]

Thacker SC, Glick SJ. Normalized glandular dose (DgN) coefficients for flat-panel CT breast imaging. Phys Med Biol. 2004; 49:5433–5444. [PubMed: 15724534]

Vedantham S, Shi L, Glick SJ, Karellas A. Scaling-law for the energy dependence of anatomic power spectrum in dedicated breast CT. Med Phys. 2013; 40:011901. [PubMed: 23298092]

Vedantham S, Shi L, Karellas A, Noo F. Dedicated breast CT: radiation dose for circle-plus-line trajectory. Med Phys. 2012a; 39:1530–1541. [PubMed: 22380385]

Vedantham S, Shi L, Karellas A, O'Connell AM. Dedicated breast CT: fibroglandular volume measurements in a diagnostic population. Med Phys. 2012b; 39:7317–7328. [PubMed: 23231281]

Zeng K, Yu H, Fajardo LL, Wang G. Cone-beam mammo-computed tomography from data along two tilting arcs. Med Phys. 2006; 33:3621–3633. [PubMed: 17089827]

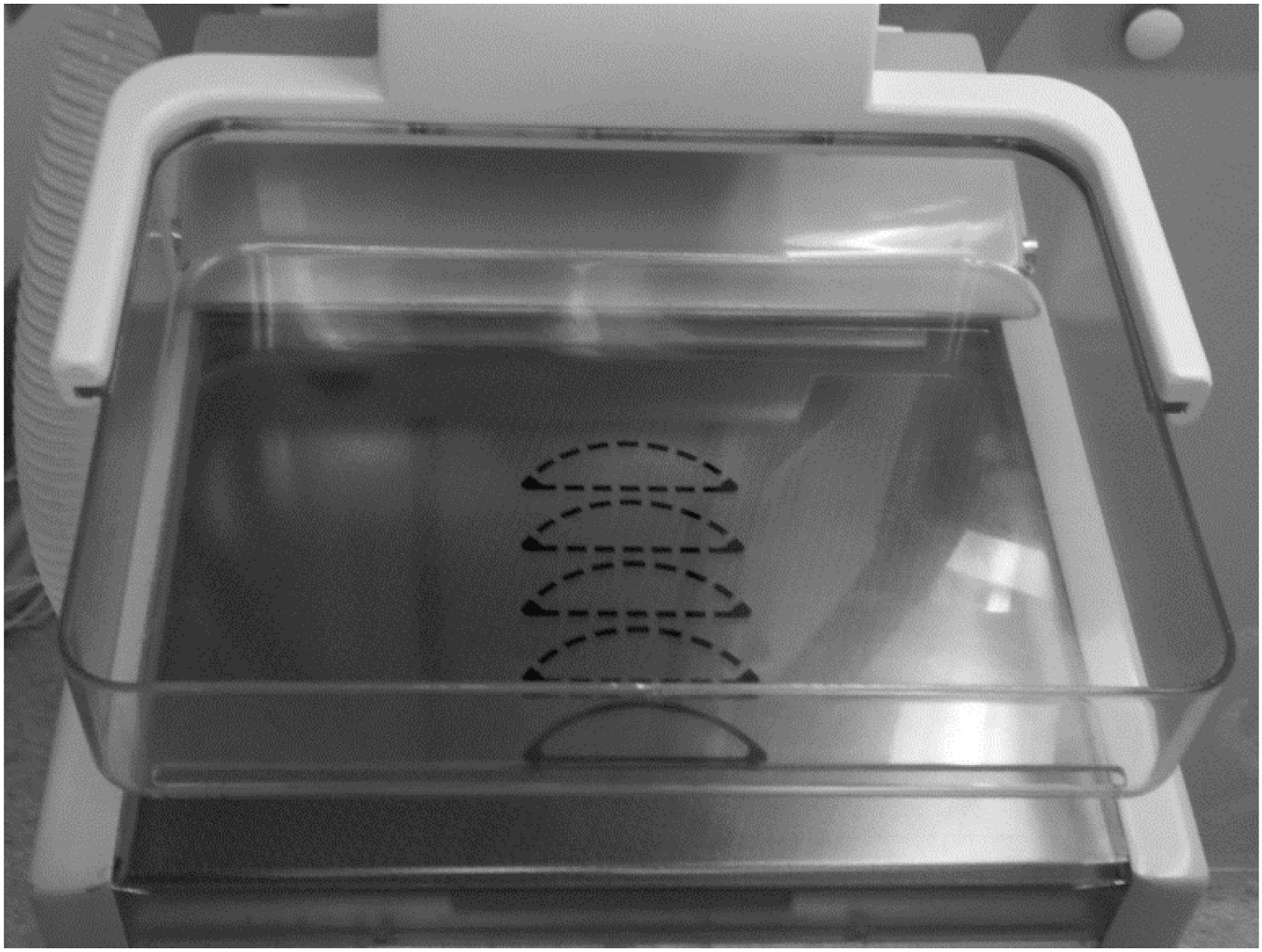

Figure 1.
Photograph of small compression paddle with a 5-mm wide slot machined at the chest-wall edge.

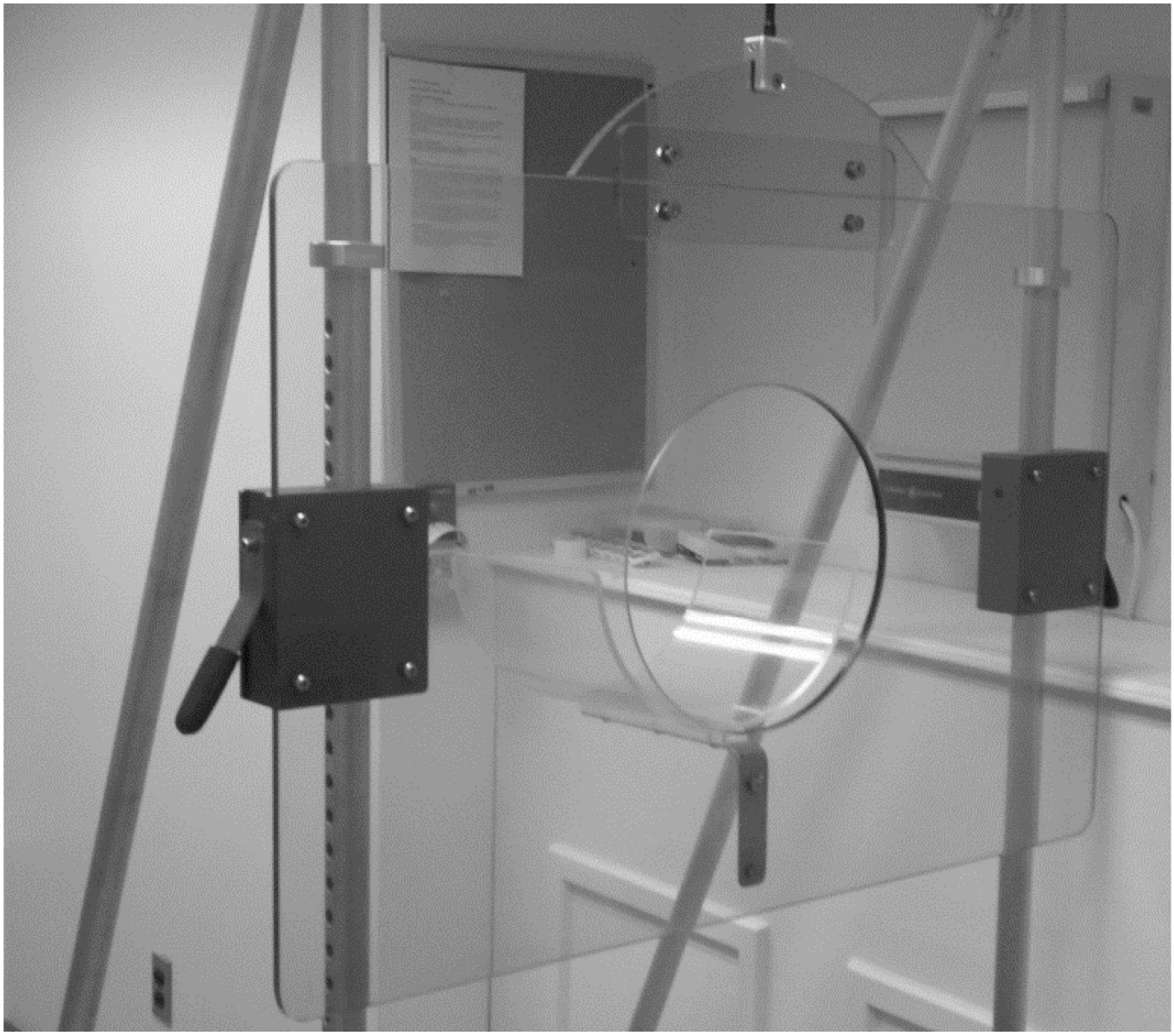

Figure 2.
Photograph of the custom-fabricated patient-protective barrier used to simulate patient positioning for an upright breast CT system.

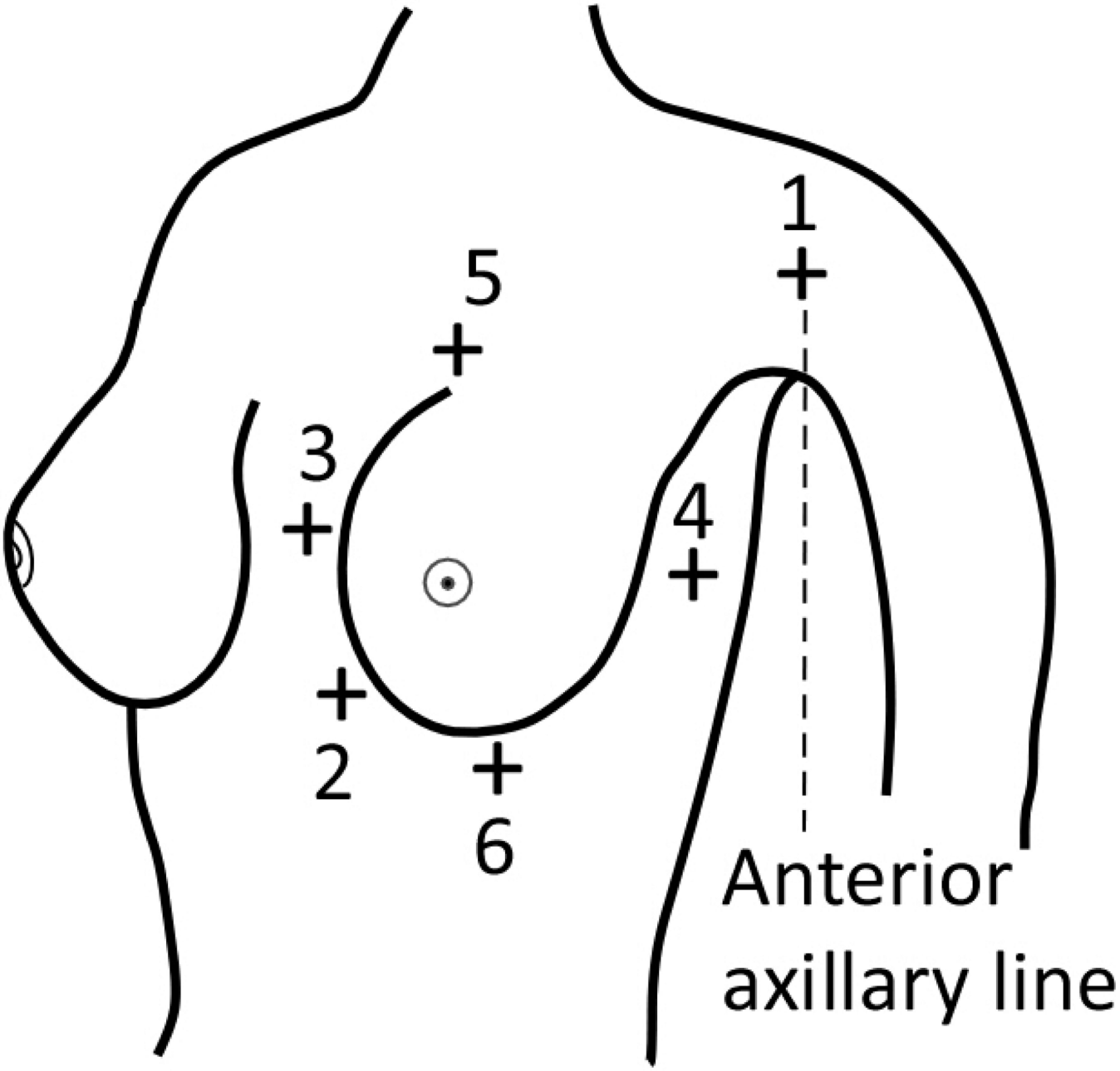

Figure 3.
Illustration (not drawn to scale) showing the locations at which breast coverage was quantified. Locations 1 through 6 correspond to: (1) anterior axillary line at the axilla; (2) medial and inferior attachment; (3) medial attachment; (4) lateral attachment; (5) superior attachment; and (6) inferior attachment.

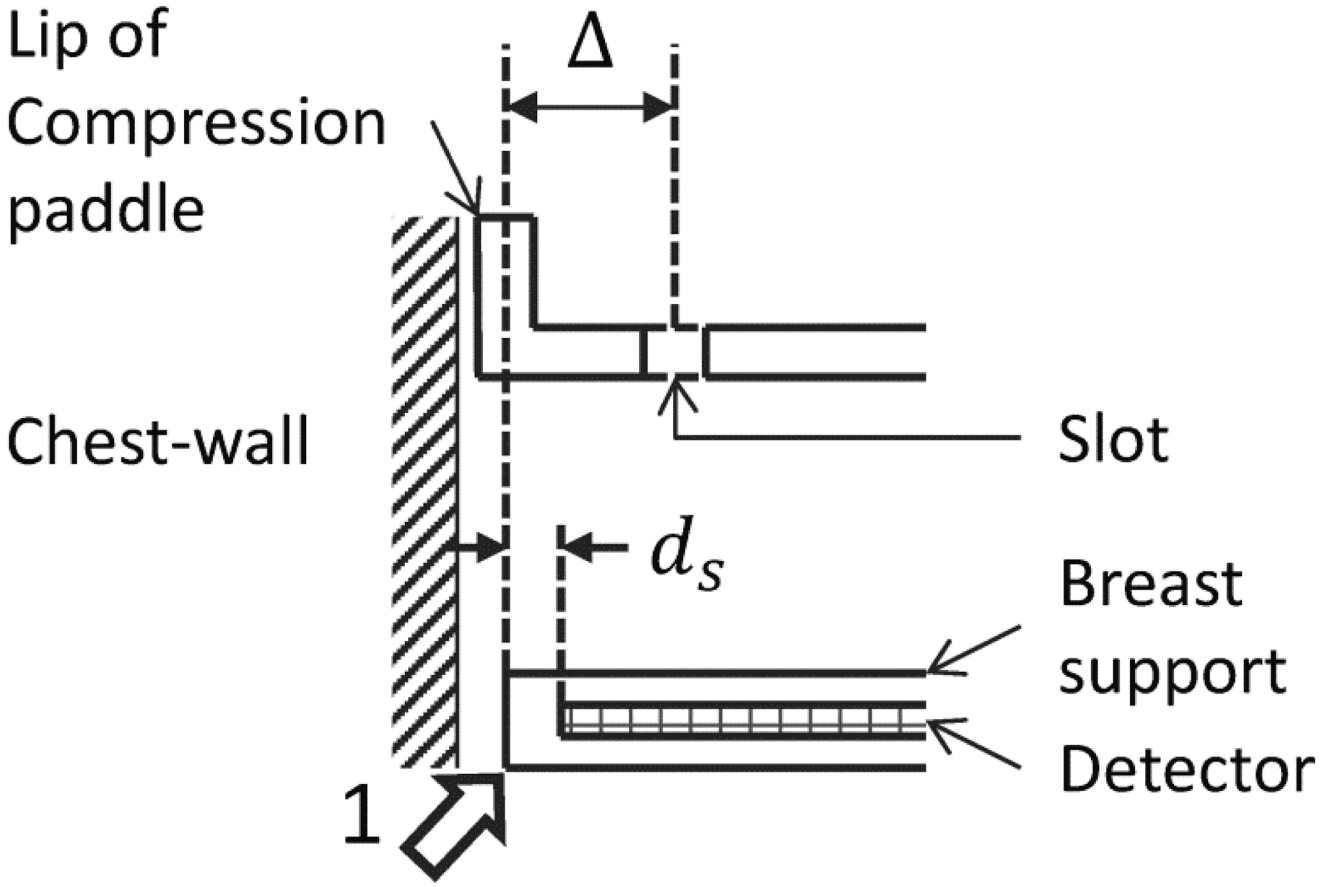

Figure 4.
Illustration (not drawn to scale) of the correction to account for the mismatch between skin marks made through the slot in the compression paddle and that made at the edge of the breast support (represented by arrow labeled 1). Skin marks corresponding to the anterior axillary line at the axilla, medial attachment and superior attachment made with the study participant positioned for mammography were corrected by $\Delta = 3$ mm to correct for the mismatch so that all locations correspond to the edge of the breast support.

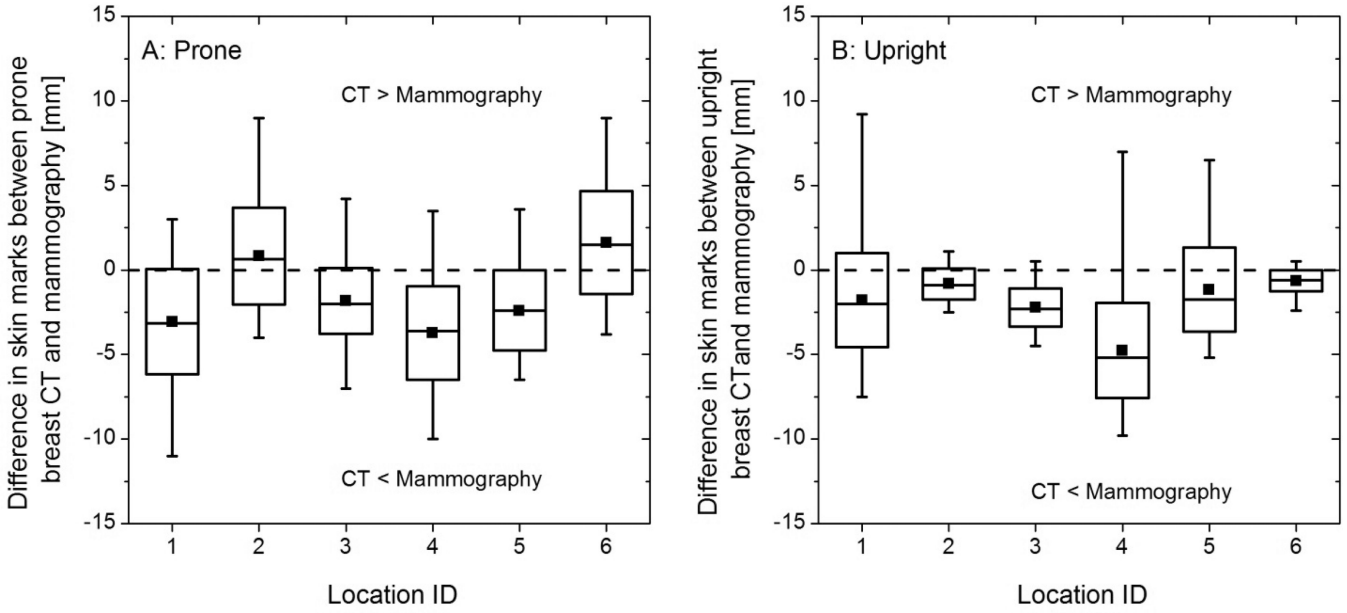

Figure 5.

Box plots of the difference in skin marks at six locations (A) between prone breast CT and mammography, and (B) between upright breast CT and mammography. The locations 1 through 6 correspond to that in Figure 3. The horizontal line within the box represents the median, the symbol within the box represents the mean, the edges of the boxes represent ±1 standard deviation from the mean, and the whiskers represent the minimum and maximum. In (A) and (B), the dashed line at $y = 0$ indicates that the skin marks from breast CT and mammography are congruent. Positive values indicate the skin mark from breast CT is posterior to mammography and negative values indicate vice versa.

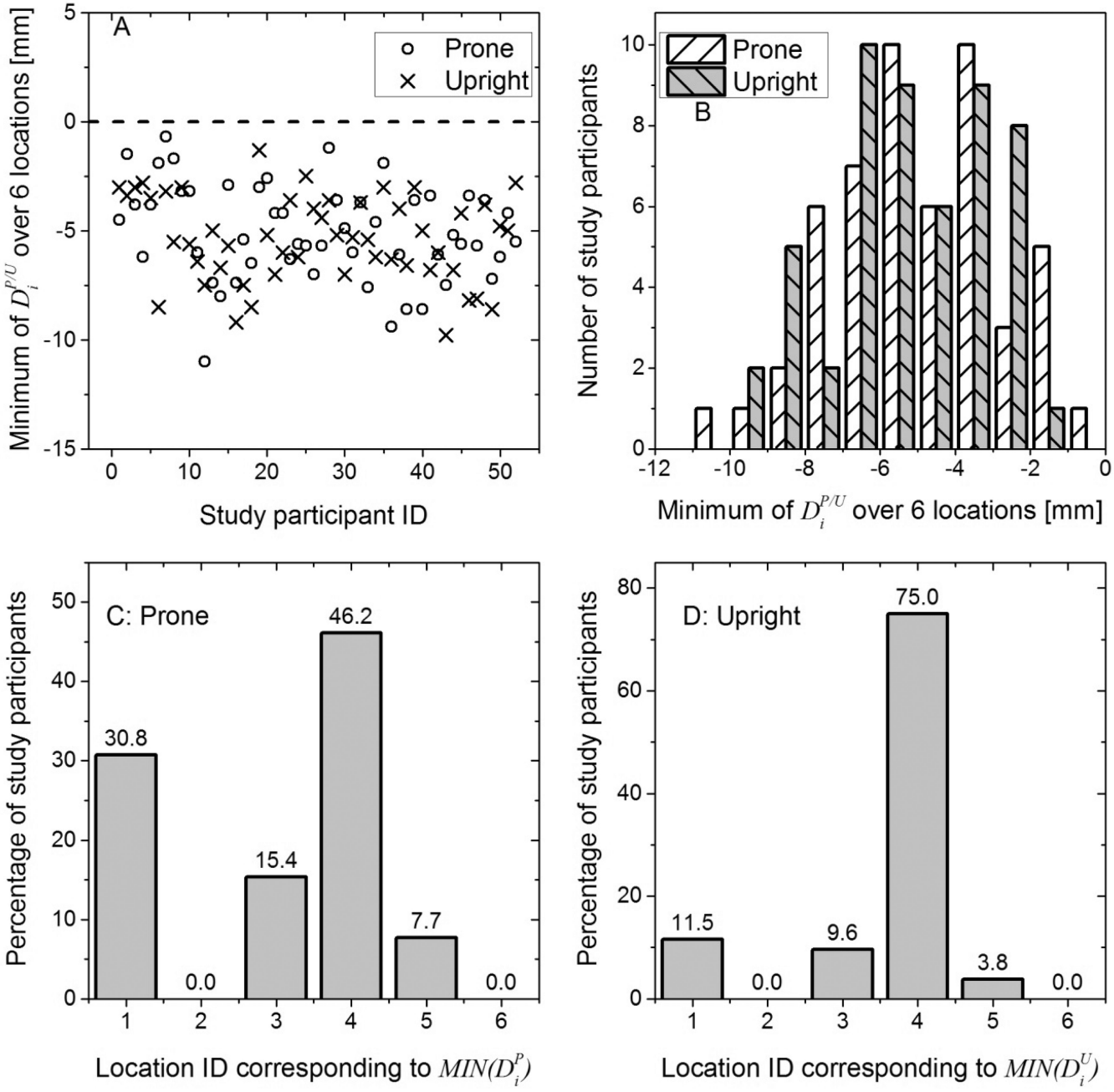

Figure 6.

In (A), the minimum of $D_i^{P/U}$ over $i = 6$ locations for each study participant is shown. For all study participants, $\underset{i}{\mathrm{MIN}}(D_i^{P/U})$ was negative indicating that the skin mark from mammography was posterior to breast CT in at least one location. In (B), the histograms of $\underset{i}{\mathrm{MIN}}(D_i^{P/U})$ are shown. At the 0.05 level, paired t-test indicated that the means of $\underset{i}{\mathrm{MIN}}(D_i^{P})$ and $\underset{i}{\mathrm{MIN}}(D_i^{U})$ were not statistically different. In (C) and (D), the histograms, expressed in percentage of study participants, of the location IDs corresponding to $\underset{i}{\mathrm{MIN}}(D_i^{P})$ and $\underset{i}{\mathrm{MIN}}(D_i^{U})$ are shown.

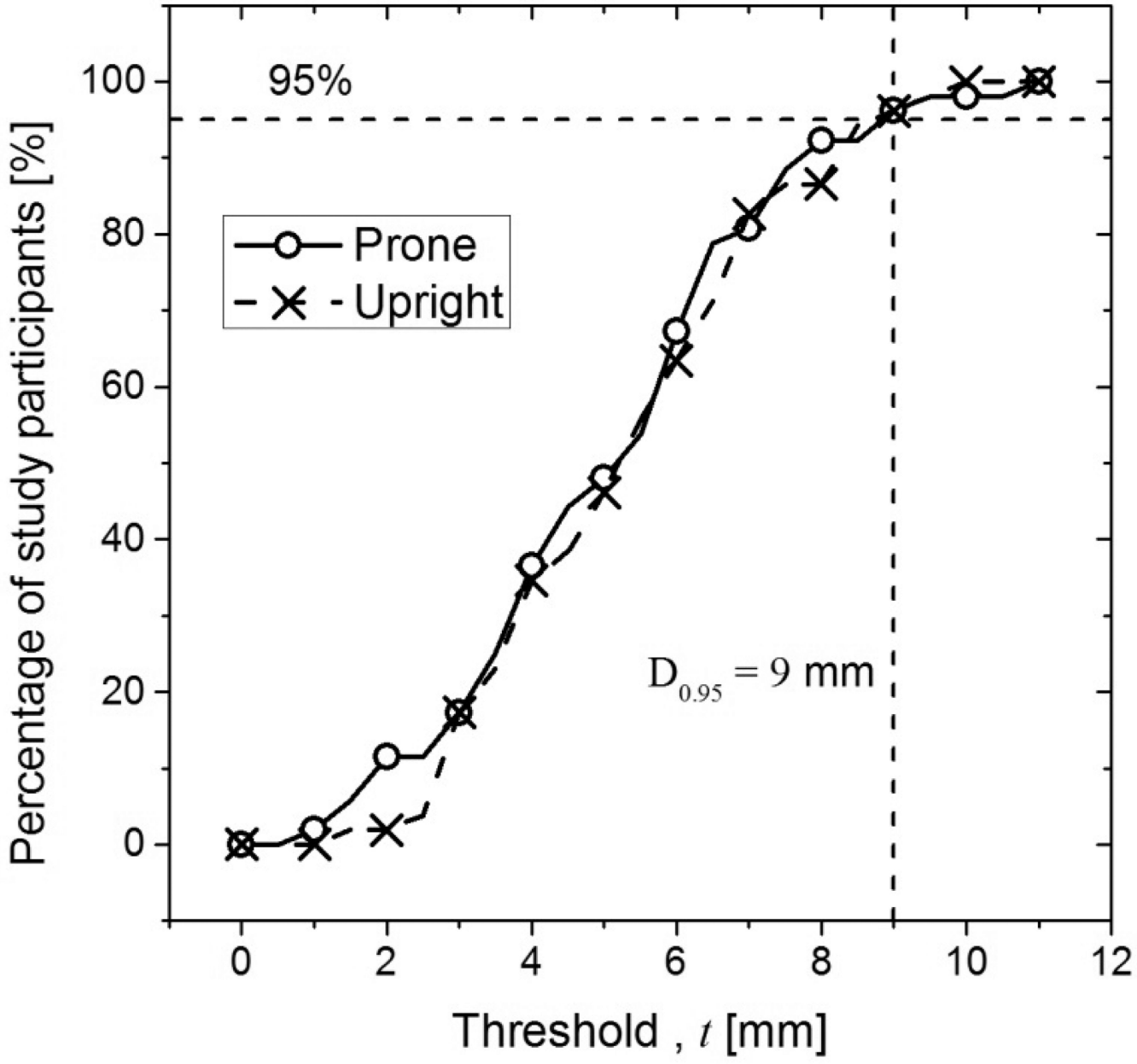

Figure 7.
The cumulative distribution shows the percentage of study participants for whom the skin mark from mammography was posterior to breast CT (prone and upright) by the specified amount (threshold, *t* in mm).

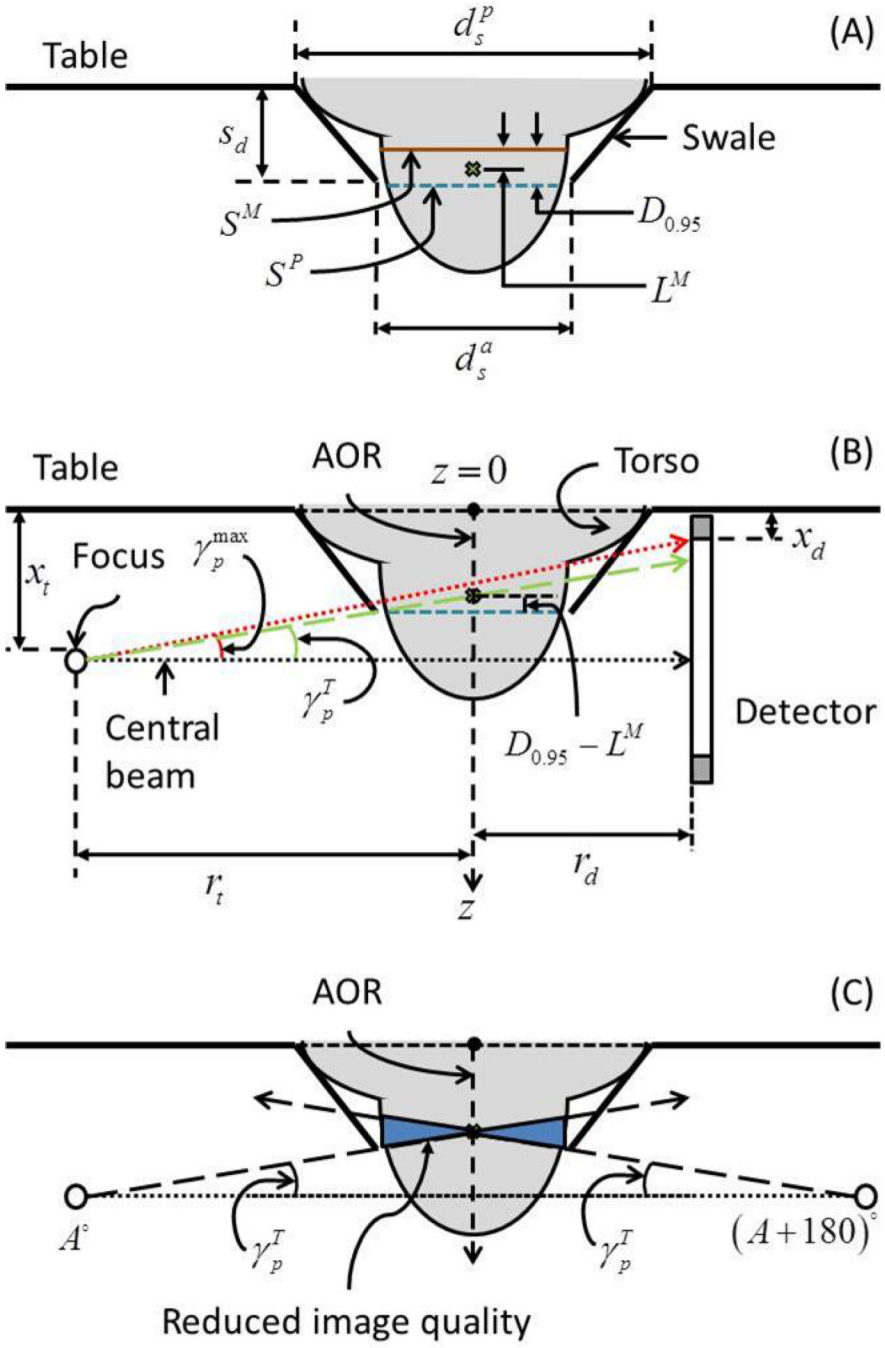

Figure 8.

Illustration of the method used to determine the optimal swale-depth in prone breast CT (not drawn to scale). In (A), the swale dimensions are shown. S^P is the skin mark with the subject positioned for prone breast CT. S^M is the skin mark along the posterior edge of the breast support with the subject positioned for mammography and is posterior to S^P by at the most 9 mm for 95% of study participants ($D_{0.95}$ =9 mm). The point marked by a cross is anterior to S^M by L^M, which is the accepted limit for chest-wall missed tissue in mammograms. In (B), γ_p^T is the cone angle needed to image through the point (marked by cross) that is posterior to

S^P by $D_{0.95}$–L^M along the axis of rotation (AOR). In (C), the breast volume where the image quality will be reduced is shown.

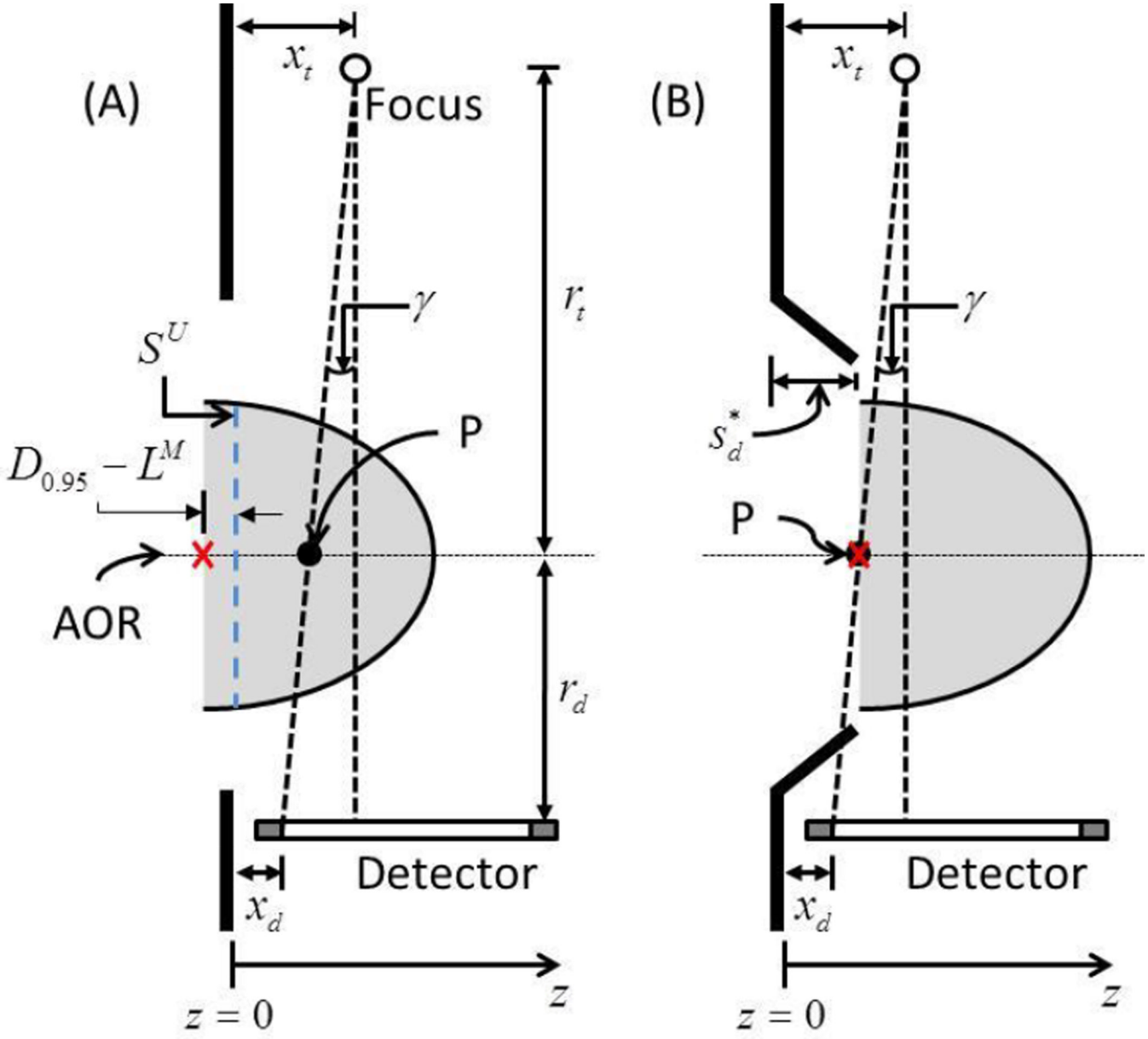

Figure 9.

Illustration of the method used to determine the optimal swale-depth in upright breast CT (not drawn to scale). The barrier used in the study had a flat surface. S^U is the skin mark with the subject positioned for upright breast CT and is aligned with the anterior surface of the barrier. $D_{0.95} - L^M$ is the amount of breast tissue posterior to S^U that needs to be imaged so as to obtain equivalent chest-wall coverage in breast CT images as mammograms for 95% of the subjects and is marked by a cross. γ is the cone angle subtended by a ray from the x-ray focal spot to the first row/column of the detector and intersects the axis of rotation at the point marked P. In (B), the swale depth needed so that the breast is shifted in the anterior direction such that the point marked by the cross is congruent with P is shown.

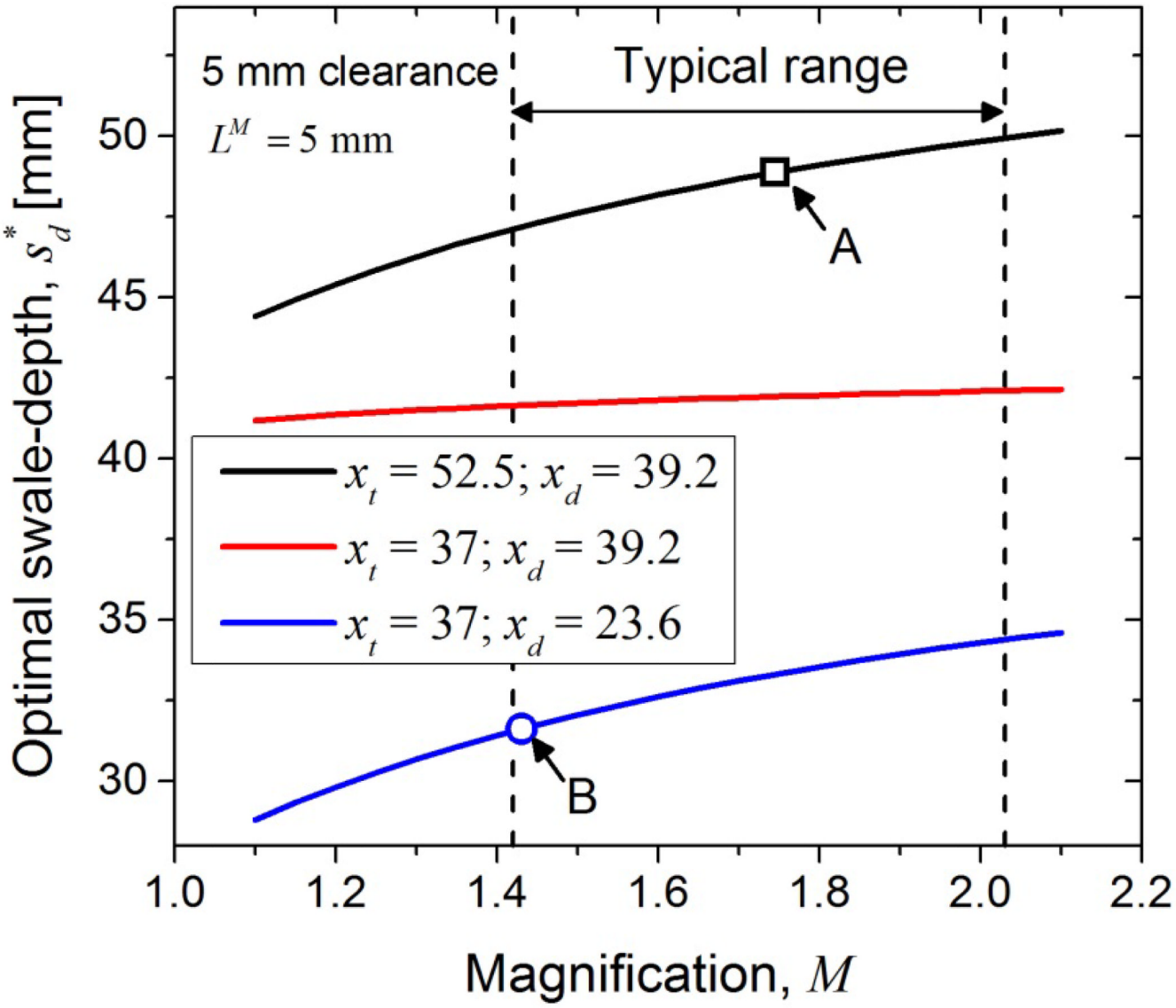

Figure 10.

The optimal swale-depth s_d^* can be reduced by decreasing magnification and by choosing x-ray tube and detector that minimize x_t and x_d, respectively. Assuming a 5 mm mechanical clearance for the x-ray tube, x_t = 52.5 mm and 37 mm, were obtained from Boone (Boone, 2004) and from specifications of M-1500 x-ray tube (Varian Medical Systems), respectively. Assuming a similar clearance for the detector, x_d = 39.2 mm and 23.6 mm, were obtained from specifications of the PaxScan® 4030CB and PaxScan® 4030MCT, respectively (Varian Medical Systems). Computations were performed assuming L^M =5 mm. The arrow labeled A indicates s_d^* for the system geometry in (Boone, 2004) and the arrow labeled B indicates s_d^* for a recently installed system at our institution.

Table 1

Race and Ethnicity characteristics

Number of subjects	**52 (100)**
Ethnic category	
Hispanic/Latino	3 (6)
Not Hispanic/Latino	49 (94)
Racial category	
American Indian/Alaskan Native	1 (2)
Asian	2 (4)
African American	1 (2)
Caucasian	46 (88)
Unknown or Not reported	2 (4)

Values in parenthesis are percentages

Table 2

Body habitus characteristics

Parameter	Mean ± S.D.	Median	Range
Age (y)	53.9 ± 7.5	52.5	40 – 73
Height (cm) †	164.5 ± 6.6	163.8	150 – 183
Circumference of chest superior to breast (cm) †	91.3 ± 8.3	90.4	60 – 109
Circumference of chest inferior to breast (cm) †	87.1 ± 8.4	86.1	73 – 106
Chin to nipple vertical distance (cm) †	28.1 ± 3.2	28	22 – 36
Nipple to umbilicus vertical distance (cm) †	18.1 ± 3.4	18.5	8 – 25

S.D. represents standard deviation

† Measurements performed with study participant standing upright

Table 3

Bra cup size and breast dimensions

	Frequently used bra cup size (participant reported)					
	A/AA	B	C	D	DD	All
n	5	14	14	15	4	52
Circumference of breast at chest-wall (cm) †						
Mean ± S.D.	40.1 ± 4.8	43.1 ± 4.9	47.1 ± 3.1	48.9 ± 4.7	52.2 ± 6.6	46.2 ± 5.5
Median	38.5	42.9	47.8	48.4	54.1	46.7
Range	35.8–48.2	35.2–51.1	40.2–51.4	40.6–57.2	42.8–57.8	35.2–57.8
Chest to nipple distance (cm) ‡						
Mean ± S.D.	6.5 ± 1.8	7.4 ± 1.6	10.2 ± 1.6	10.9 ± 1.3	11.7 ± 1.3	9.4 ± 2.3
Median	6.2	7.3	9.9	10.6	12.3	9.7
Range	5.0–9.4	4.0–9.7	8.0–13.0	9.2–13.5	9.8–12.5	4.0–13.5

S.D. represents standard deviation

† Measurements performed with study participant standing upright

‡ Measurement performed with breast supported on a mammography unit and without compression

Table 4

Correlation (Spearman *rho*) between breast dimensions and body habitus measures

	Circumference of breast at Chest-wall	Height	Chin to nipple vertical distance	Nipple to umbilicus vertical distance	Chest to nipple distance	Circumference of chest superior to breast	Circumference of chest inferior to breast
Circumference of breast at Chest-wall	1	−0.125	0.242	0.258	0.485*	0.424*	0.484*
Chest to nipple distance	0.485*	−0.019	0.706*	−0.068	1	0.505*	0.601*

*indicates statistically significant correlation at the 0.05 level (2-tailed test)

Table 5

Correlation (Spearman *rho*) between body habitus measures and location-dependent posterior breast tissue available for imaging with prone and upright breast CT

	Anterior axillary line at the axilla	Medial and inferior attachment	Medial attachment	Lateral attachment	Superior attachment	Inferior attachment
Prone positioning of study participants						
Circumference of breast at chest-wall	−0.222	−0.176	−0.271	−0.280*	−0.298*	−0.224
Chin to nipple vertical distance	−0.052	−0.090	−0.110	−0.071	−0.083	0.057
Nipple to umbilicus vertical distance	0.157	0.120	−0.058	−0.070	0.098	−0.026
Chest to nipple distance	−0.137	0.029	0.037	−0.063	−0.247	0.041
Circumference of chest superior to breast	−0.099	0.099	0.140	−0.039	−0.264	0.146
Circumference of chest inferior to breast	−0.123	0.053	0.050	−0.173	−0.366*	0.091
Upright positioning of study participants						
Circumference of breast at chest-wall	−0.242	−0.032	−0.102	−0.153	−0.263	0.144
Chin to nipple vertical distance	−0.027	−0.306*	−0.294*	−0.010	0.008	−0.025
Nipple to umbilicus vertical distance	0.036	0.293*	0.043	−0.232	0.091	0.095
Chest to nipple distance	−0.209	−0.199	−0.156	−0.124	−0.207	0.037
Circumference of chest superior to breast	−0.239	0.090	−0.188	−0.213	−0.259	0.182
Circumference of chest inferior to breast	−0.100	0.089	−0.263	−0.214	−0.250	0.208

*indicates statistically significant correlation at the 0.05 level (2-tailed test)

Phys Med Biol. Author manuscript; available in PMC 2014 June 21.

Table 6

Correlation (Spearman *rho*) between locations for posterior tissue available for imaging with prone and upright breast CT

	Anterior axillary line at the axilla	Medial and inferior attachment	Medial attachment	Lateral attachment	Superior attachment	Inferior attachment
Prone positioning of study participants						
Anterior axillary line at the axilla	1	0.177	0.077	0.496*	0.759*	0.371*
Medial and inferior attachment	0.177	1	0.755*	0.230	0.335*	0.710*
Medial attachment	0.077	0.755*	1	−0.002	0.271	0.564*
Lateral attachment	0.496*	0.231	−0.002	1	0.365*	0.382*
Superior attachment	0.759*	0.335*	0.271	0.365*	1	0.386*
Inferior attachment	0.371*	0.710*	0.564*	0.382*	0.386*	1
Upright positioning of study participants						
Anterior axillary line at the axilla	1	0.029	−0.011	0.218	0.664*	0.115
Medial and inferior attachment	0.029	1	0.167	−0.030	0.072	0.396*
Medial attachment	−0.011	0.167	1	−0.197	0.160	−0.079
Lateral attachment	0.218	−0.030	−0.197	1	0.080	−0.095
Superior attachment	0.664*	0.072	0.160	0.080	1	0.020
Inferior attachment	0.115	0.396*	−0.079	−0.095	0.020	1

*indicates statistically significant correlation at the 0.05 level (2-tailed test)

Table 7

Correlation (Spearman *rho*) between body habitus measures and maximum reduction in chest-wall tissue available for imaging with prone and upright breast CT

	$\min_i(D_i^P)$	$\min_i(D_i^U)$
Circumference of breast at chest-wall	−0.351*	−0.136
Chin to nipple vertical distance	−0.005	0.008
Nipple to umbilicus vertical distance	0.055	−0.250
Chest to nipple distance	−0.159	−0.126
Circumference of chest superior to breast	−0.219	−0.253
Circumference of chest inferior to breast	−0.277*	−0.217

*indicates statistically significant correlation at the 0.05 level (2-tailed test)